

# Adsorption of polyampholytes on charged surfaces

Florian Ozon<sup>a</sup>, Jean-Marc diMéglio<sup>b</sup>, and Jean-François Joanny<sup>c</sup>

Institut Charles Sadron (CNRS UPR 022), 6 rue Boussingault, 67083 Strasbourg Cedex, France

Received: date / Revised version: date

**Abstract.** We have studied the adsorption of neutral polyampholytes on model charged surfaces that have been characterized by contact angle and streaming current measurements. The loop size distributions of adsorbed polymer chains have been obtained using atomic force microscopy (AFM) and compared to recent theoretical predictions. We find a qualitative agreement with theory; the higher the surface charge, the smaller the number of monomers in the adsorbed layer, in agreement with theory. We propose an original scenario for the adsorption of polyampholytes on surfaces covered with both neutral long-chain and charged short-chain thiols.

**PACS.** 82.37.Gk STM and AFM manipulations of a single molecule { 82.35.Gh Polymers on surfaces; adhesion

## 1 Introduction

The study of the adsorption of charged polymers on charged surfaces is of great interest in both polymer physics and industrial practice. A better understanding of the adsorption phenomenon has already led to numerous applications related to wetting, lubrication, adhesion :: Poly-electrolytes are for instance currently used to control the colloidal stability of dispersions or in waste water treatment. Relatively few experimental studies have however been performed on polyampholyte adsorption. Polyampholytes are polymers carrying both positive and negative charges along the same chain [1,4]. On the theoretical side, Dobrynin, Rubinstein and Joanny have recently proposed a new adsorption mechanism induced by the polarization of the chains in the electric field of the surface [5].

The present work aims at comparing theory and experiments by characterizing adsorbed polyampholyte layers on controlled charged surfaces with atomic force microscopy (AFM). Section 2 presents the experimental procedures: the fabrication of the charged surfaces by reaction of neutral and charged thiols on gold-coated substrates, the AFM experiments and the two characterization techniques of the surfaces, contact angle and streaming current measurements. Section 3 summarizes the theory of polyampholyte adsorption: the case of a single chain [5]

has been extended to the case of a solution [6] and the monomer concentration profile allows us to derive the theoretical loop size distribution in the adsorbed layer. In Section 4, the experimental loop size distribution is compared to theory and qualitative agreement is found. Contact angle and electrokinetics measurements are interpreted in the light of the AFM results.

## 2 Experimentals

### 2.1 Surface preparation

The charged surfaces have been prepared as described in [7]. Substrates were cleaved mica for AFM experiments and contact angle measurements, or microscope glass slides for streaming current measurements. The gold-coated surfaces have been realized under high vacuum by deposition of 5 nm of chromium, which acts as a wetting agent, followed by 50 nm of gold. The surfaces are then left about 20 hours in an ethanol:millicolar solution of thiols. We have used  $\text{HS}-(\text{CH}_2)_2-\text{SO}_3^- \text{Na}^+$ ,  $\text{HS}-(\text{CH}_2)_2-\text{CH}_3$  (both purchased from Aldrich) and  $\text{HS}-(\text{CH}_2)_2-(\text{CF}_2)_7-\text{CF}_3$  (kindly provided by Marie-Pierre Krafft from ICS-Strasbourg). The surface charge is changed by mixing charged and neutral thiols in varying proportions. Table 1 gives their respective lengths when the aliphatic (or uorinated) chain is extended.

### 2.2 Polyampholyte adsorption

The polyampholyte has been synthesized by microemulsion-polymerization by S. Neyret [8] from a neutral monomer,

<sup>a</sup> Present address: Laboratoire de Dynamique des Fluides Complexes (Université Louis Pasteur – CNRS UMR 7506), 3, rue de l'Université, 67084 Strasbourg Cedex, France

<sup>b</sup> Université Louis Pasteur and Institut Universitaire de France

<sup>c</sup> Present address: Physico-Chimie Curie (Institut Curie – CNRS UMR 168), 11 rue Pierre et Marie Curie, 75231 Paris Cedex 05, France

Thiol	Size (nm)
$\text{HS}-(\text{CH}_2)_2-\text{SO}_3$	0.6
$\text{HS}-(\text{CH}_2)_2-\text{CH}_3$	0.6
$\text{HS}-(\text{CH}_2)_2-(\text{CF}_2)_7-\text{CF}_3$	1.5

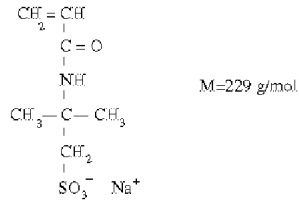
Table 1. Lengths of thiols in all-trans conformations

acrylamide, and two charged monomers, sodium 2-(acrylamido)-2-methylpropanesulfonate (AMPSNa) and [2-(methacryloxy)ethyl]trimethylammonium chloride (MADQUAT). The chemical formulae are shown on Figure 1. The total

## 1) Acrylamide



## 2) AMPSNa : sodium 2-(acrylamido)-2-methylpropanesulfonate



## 3) MADQUAT : [2-(methacryloyloxy)ethyl]trimethylammonium chloride

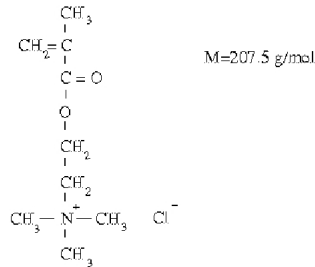


Fig. 1. Chemical formulae of the monomers used for polyampholyte synthesis.

number of monomers in the polymer is  $\sim 4 \cdot 10^4$ ; its composition (93.5/3.75/3.75 % in acrylamide/AMPSNa/MADQUAT) has been determined by elementary chemical analysis and shows that the polyampholyte is globally electrically neutral. The experimental determination of reactivity ratios has shown that polymerization in microemulsion leads to an almost random distribution of monomers along the chain [8]. This is due to the strong concentration of counterions in the microemulsion droplets (diameter  $\sim 50$ -100 nm) that strongly screens the electrostatic interactions between charged monomers. However, because of

the different reactivity ratios of the monomers, the fluctuations of the net charge of the polyampholytes (defined as the sum of all the charges along the chain), are larger than predicted for a perfectly random distribution [9]. After the synthesis, the counterions are removed by dialysis against pure water. The polyampholyte solution has been prepared by dissolving 10 mg of polymer in 100 g of a NaCl aqueous solution (concentration  $0.15 \text{ mol l}^{-1}$ ), the polymer being insoluble in pure water and the critical salt concentration to reach solubility, as determined in [10], being  $0.1 \text{ mol l}^{-1}$ . The thiolated surfaces have been left in the polyampholyte solution for one hour; this was long enough for the polymer to adsorb. After that, the surfaces have been rinsed with milli-Q water before being used in the AFM experiments. While salt is needed in bulk solution to ensure that polyampholyte chains do not collapse, the electric field of a charged substrate should be sufficient to stretch adsorbed chains (cf Fig. 5) and avoid their collapse; loops of adsorbed polyampholyte can then develop in milli-Q (de-ionized) water. This has been addressed theoretically in [11] where it is suggested that the behaviour of an adsorbed polyampholyte is similar to the behaviour of an adsorbed soluble polymer. Throughout our study, we consider water as a  $\theta$ -solvent for the polyampholyte; water is indeed close to  $\theta$ -solvent for polyacrylamide (the second virial coefficient  $A_2$  for a polyacrylamide with a molar mass equal to  $4.7 \cdot 10^6 \text{ g mol}^{-1}$  is low:  $A_2 = 0.64 \cdot 10^{-4} \text{ mol cm}^3 \text{ g}^{-2}$  [12]) and the used polyampholyte is mostly composed of acrylamide.

## 2.3 AFM experiments

A Digital Instruments Nanoscope III force microscope has been used, fitted with its standard fluid cell. For each experiment, a new cantilever was cleaned in a water plasma [13]. Cantilever spring constants (from Digital Instruments specifications) were  $0.05 \text{ N m}^{-1}$  for experiments on  $\text{HS}-(\text{CH}_2)_2-\text{SO}_3$  /  $\text{HS}-(\text{CH}_2)_2-\text{CH}_3$  surfaces and  $0.03 \text{ N m}^{-1}$  for experiments on  $\text{HS}-(\text{CH}_2)_2-\text{SO}_3$  /  $\text{HS}-(\text{CH}_2)_2-(\text{CF}_2)_7-\text{CF}_3$  surfaces. Milli-Q water ( $\text{pH} = 5.7$ ) is injected in the liquid cell set-up and we have then waited half an hour to start the AFM force measurements. The tip-surface then underwent repeated approach-separation cycles at 1 Hz frequency; beyond this value, hydrodynamic forces appear. In de-ionized water ( $\text{pH} = 5.7$ ), the total salt concentration ( $\text{H}_3\text{O}^+$  and  $\text{HCO}_3^-$ ) is  $4 \cdot 10^{-6} \text{ mol l}^{-1}$ , which corresponds to a Debye length  $\lambda_D = 150 \text{ nm}$ . The thickness of the adsorbed layer predicted by theory being roughly  $\lambda_D$  in the pseudo-brush regime, a z-displacement of the piezoelectric system much larger than this length was chosen, namely 500 nm, which allows to determine precisely the force profile over a 400 nm range.

A peak sometimes appears on the force curves and is understood as the detachment of a loop that bridged tip and substrate [14, 15] (Figure 2). Some extension curves have been fitted using the Freely Jointed Chain [16] and the Worm Like Chain [17] models and the extension of the loop at the detachment was always found above 90 % of

the contour length; the detachment distance of the loop can be considered as its contour length.

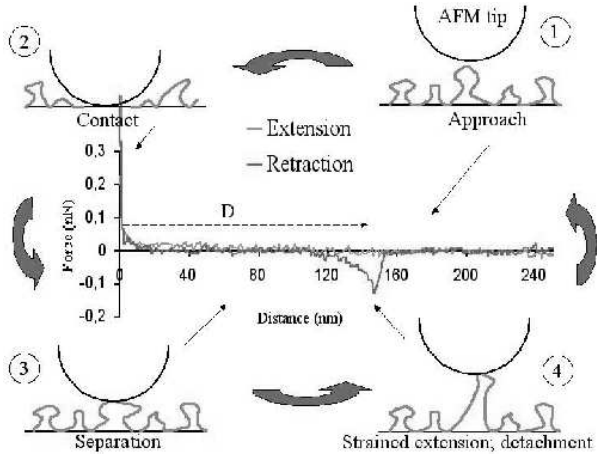


Fig. 2. Schemes showing a possible path to the formation and extension of a connective bridge (after [14]); corresponding force curve.

For each AFM experiment, more than two hundred jumps have been collected to obtain the loop size distribution. The data have been analyzed using the method introduced in [14] for the adsorption of polydimethylsiloxane on silica, and later used to investigate the adsorption layers of polyacrylamide derivatives [15]. The loop size distribution  $S(n)$  (defined as the probability for a loop to have  $n$  monomers) is deduced from the distribution  $p(D)$  of detachment distances  $D$  via the relation  $S(n)dn = p(D)dD$  and the hypothesis that  $D \propto na$  where  $a$  is the Kuhn length. Assuming that the experimental situation corresponds to the fence regime defined in Section 3 and using Eq. (13), the distribution  $p(D)$  is fitted by:

$$p(D) = A D^{1-2} (D + h)^{-1} \quad (1)$$

$A$  is a numerical prefactor and the number  $g$  of monomers in a chain section with a size of the order of the layer of thickness  $h$  (the Gouy-Chapman length, see Section 3) is given by  $h = a$ . Values of  $D$  lower than 20 nm have not been taken into account in the fit because of a lower resolution near the surface and the presence of a primary adhesion peak (due to van der Waals interactions) on some force curves.

## 2.4 Contact angle measurements

Contact angles of a water sessile drop have been measured using an optical microscope. The surfaces were tilted until the drop moved, defining both advancing  $\theta_a$  and receding  $\theta_r$  angles. Because of the Young-Dupr  relation  $\gamma_{LV} \cos \theta = \gamma_{SV} - \gamma_{SL}$ , where  $\gamma_{LV}$ ,  $\gamma_{SV}$  and  $\gamma_{SL}$  are respectively the interfacial free energies of the liquid-vapour, solid-vapour and solid-liquid interfaces,  $\cos \theta$  was plotted against the ratio of charged thiols to (charged +

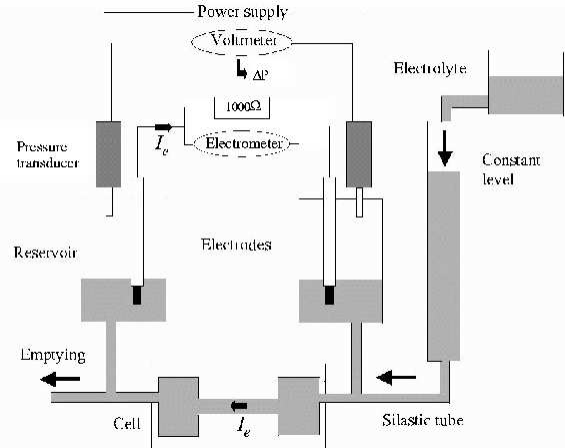


Fig. 3. Schematic set-up for streaming current measurements.

uncharged) thiols. Indeed, for a given liquid/vapour couple (here water/air),  $\cos \theta$  should approximately vary linearly with the solid surface composition if there is neither segregation of the thiols at the surfaces nor special conformational effects of the thiols. The contact angle hysteresis ( $\cos \theta_r - \cos \theta_a$ ) also gives some insight on the surface heterogeneities [18][20].

## 2.5 Electrokinetic measurements

An original apparatus to measure the streaming current of planar substrates has been designed and is schematically represented on Figure 3. Figure 4 shows a detailed view of the measurement cell.

The measurement cell is built from two PMMA plastic blocks that comprise an accurately cut depression to fit in two test glass slides of dimensions  $7.5 \times 2.5 \times 0.1$  cm<sup>3</sup>. Each slide is firmly held in position by two Viton rubber stops. A small reservoir was machined at each extremity of the base block. The two blocks are separated by a Teflon (PTFE) gasket of 0.02 cm thickness, aligned with stainless steel pegs. A capillary of dimension  $7.5 \times 2.2 \times 0.02$  cm<sup>3</sup> is then formed between the two slides by clamping together the two blocks with 8 screws. The principle of the measurement is the following: upstream, an electrolyte solution ( $10^{-3}$  mol l<sup>-1</sup> KCl at pH = 5.7) falls into a column so that the level of the liquid remains constant, which ensures a constant pressure difference  $\Delta p$  between the two extremities of the measurement cell;  $\Delta p$  is measured via two Kobold pressure transducers ( $0$ – $10^4$  Pa) linked to tightly closed reservoirs. The measured pressure difference accuracy is 5 Pa. The streaming current is measured with a Keithley 617 electrometer (impedance  $2 \times 10^{14}$  M $\Omega$ ) used as a nano-ammeter connected to two silver electrodes placed in each reservoir of the measurement cell. The electrodes were covered with silver chloride by electrolysis to prevent their polarization.

The principle of the potential determination has been discussed by Hurd and Hackerman [21] in their study of metals (Au, Ag and Pt) in aqueous solutions. In order to

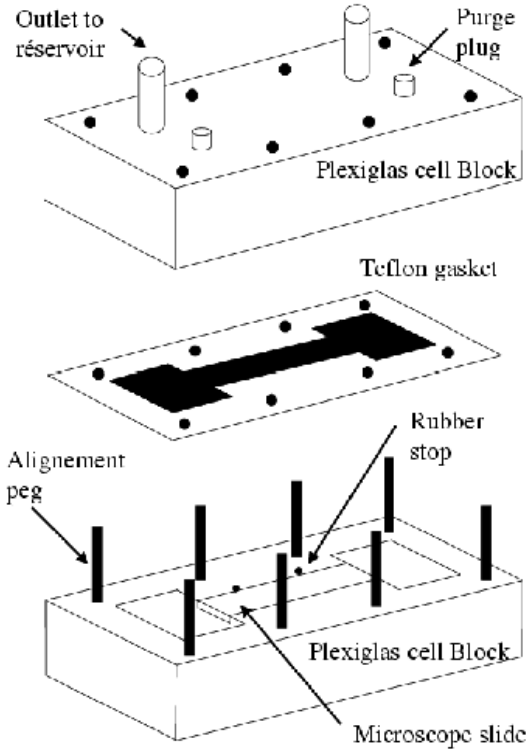


Fig. 4. Detailed view of the measurement cell.

to measure the streaming current, we have used a shunt resistance of  $10^3 \Omega$ ; the measured impedance of the capillary tube is  $1 M\Omega$  which ensured that the measured current did not depend on the value of the shunt resistance [21].

In the case of a laminar and established flow across a charged capillary of length  $L$ , width  $l$  and height  $h$ , the potential can be calculated from the pressure  $p$  dependence on the streaming potential  $U_s$  and the streaming current  $I_s$  (Smoluchowski equations [22]):

$$(U_s) = \frac{1 + \frac{2\sigma_s}{h}}{\eta} \frac{dU_s}{d(p)} \quad (2)$$

$$(I_s) = \frac{L}{\eta} \frac{dI_s}{d(p)} \quad (3)$$

where  $(U_s)$  is the potential calculated from the streaming potential,  $(I_s)$  the potential obtained from the streaming current,  $\eta$  the viscosity,  $\epsilon$  the permittivity of the uid,  $\sigma_1$  the liquid (electrolyte) conductivity and  $\sigma_s$  the surface conductivity. If the influence of the interfacial conductivity is not considered, only an apparent potential is determined from the streaming potential which is lower than the actual one. The potential determined from the streaming current, however, is independent of the surface conductivity and is a function only of the channel geometry for a given electrolyte. The thiolated gold surfaces are

a priori conducting and we have then chosen to deduce from streaming current measurements.

### 3 Theory

We summarize in this section the theory of polyampholyte adsorption in a  $\gamma$ -solvent [5,6] that we need to derive the loop size distributions. We also give numerical estimates of the various threshold values using the characteristics of the polyampholyte chains used in our experimental study and described in Section 2 ( $N$ , number of monomers  $\approx 4 \cdot 10^4$ ;  $f$ , fraction of charged monomers  $\approx 0.075$ ;  $a$ , monomer size  $\approx 0.3$  nm;  $R_0$ , ideal (Gaussian) chain size  $\approx 60$  nm).

#### 3.1 Single chain adsorption [5]

In the Poisson-Boltzmann approximation, a charged surface (of surface charge density  $\sigma_0$ ), immersed in a solvent of dielectric permittivity  $\epsilon$ , in absence of added salt, generates an electric field  $E(z)$  at a distance  $z$  from the surface:

$$E = \frac{e \sigma_0}{\epsilon (1 + z/\lambda_D)} \quad (4)$$

where  $\lambda_D$  is the so-called Gouy-Chapman length which gives the thickness of the counterion layer close to the surface [23]:

$$\lambda_D = \frac{1}{2 \sigma_0 l_B} \quad (5)$$

with  $l_B$  the Bjerrum length  $l_B = e^2 / (4 \pi \epsilon k_B T)$  ( $e$  is the elementary charge and  $k_B T$  the thermal energy,  $l_B \approx 7$  Å in pure water).

Because of the statistical distribution of the charges along the chain, the two halves of a neutral chain carry opposite charges of order  $(fN)^{1/2}e$ . The electric field can polarize a neutral polyampholyte chain which behaves as a dipole (of size  $R_z$  and charge  $e(fN)^{1/2}$ ) and is then attracted by the charged surface. In a  $\gamma$ -solvent of the polymer backbone, the chain is stretched when  $R > N^{1/2}a$ ; this corresponds to a threshold field  $E_1 \approx 1/(N^{1/2}a) (k_B T/e) (fN)^{1/2}$ .

Three regimes of adsorption have been predicted depending on the charge density  $\sigma_0$  (Figure 5).

i) pole regime ( $\sigma_0 < aN^{1/2}$ ). A chain is stretched when  $E > E_1$ ; the corresponding surface charge density and Gouy-Chapman length are respectively  $\sigma_1 \approx (fN)^{1/2} (l_B R_0)^{-1}$  and  $\lambda_1 \approx R_0 (fN)^{1/2}$ . For the polyampholyte studied in the experiment, we get  $\sigma_1 \approx 6.9 \cdot 10^{13}$  charges/m<sup>2</sup> and  $\lambda_1 \approx 3290$  nm. Beyond this threshold, the chain size  $R_z$  in the direction normal to the surface grows linearly with charge density as  $R_{00} = \lambda_1$ :

ii) fence regime. The Gouy-Chapman length becomes comparable with  $R_z$  when  $\sigma_0 \approx \sigma_2 \approx (fN)^{1/4} (l_B R_0)^{-1}$ . Because of the screening of the electric field by the counterions, the chain then remains confined within a slice of

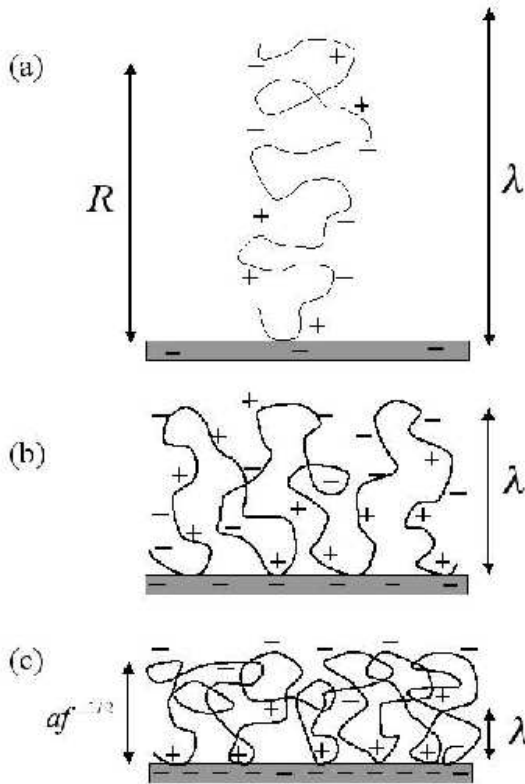


Fig. 5. Schematic sketch of the configurations of a polyampholyte chain near a charged surface: (a) the pole regime; (b) the fence regime; (c) the pancake regime.

height (for our system,  $\sigma_2 \approx 5.2 \cdot 10^{14}$  charges/m<sup>2</sup> associated with a Gouy-Chapman length  $\lambda_2 \approx 440$  nm). An adsorbed chain can be divided into subunits (blobs) of size  $a$ . The number  $g$  of monomers per blob is obtained by considering each subunit as an independent chain:

$$g = f^{1/3} (\lambda_B a_0)^{4/3} \quad (6)$$

Each blob carries an induced dipole moment  $e f^{1/2} g^{1/2}$ .

iii) pancake regime. The polyampholyte chain is strongly bound to the surface when the adsorption energy of each blob of size  $a$  is larger than the thermal energy  $k_B T$ . This happens for a charge density  $\sigma_0$  larger than  $\sigma_3 \approx f^{1/2} = (a \lambda_B)^{-1}$ . The condition  $\sigma_0 > \sigma_3$  then defines the pancake regime: the Gouy-Chapman length  $\lambda_0$  is smaller than the mean-square distance between charged monomers  $a f^{1/2}$  ( $\sigma_3 \approx 2.3 \cdot 10^{17}$  charges/m<sup>2</sup> and  $\sigma_3 \approx 1$  nm in our experimental situation). Monomers with charge opposite to the surface charge are in contact with the surface while the other monomers form loops dangling in solution at distances  $z > a$ . The average size of these loops can be estimated from the balance between the electrostatic force acting on the monomers  $e^2 \sigma_0 = (e^2 / z) / k_B T = z$  and the elastic force  $k_B T z f = a^2$  needed to stretch a chain with  $f^{1/2}$  monomers; the thickness of the adsorbed layer is then approximately  $a f^{1/2}$ . It is interesting to note that this thickness does not depend on the surface charge  $\sigma_0$ .

### 3.2 Multichain adsorption [6]

The previous model has been extended to the case of multichain adsorption by Dobrynin and co-workers [6].

i) multilayers of stretched chains ( $\sigma_1 < \sigma_0 < \sigma_2$ , Figure 6a).

The predicted monomer concentration profile is:

$$c(z) \approx c_0 \frac{1}{1 + z/\lambda} \quad (7)$$

where  $c_0 = a^{-3} N^{1/2}$  is the overlap concentration. At distances  $z > \lambda$ , a hyperbolic density profile  $c(z) \approx c_0 \lambda/z$  is expected. Near the surface, the polymer density saturates at  $c(0) \approx c_0 \lambda$ . The crossover between semi-dilute and dilute regimes of the adsorbed chains occurs at distance  $z \approx \lambda$  where the attractive interaction between each chain and the surface compares to  $k_B T$ :  $\lambda$  can be considered as the thickness of the adsorbed layer.

ii) self-similar stretched pseudo-brush ( $\sigma_2 < \sigma_0 < \sigma_3$ , Figure 6b).

The size of the chains in the first adsorbed layer saturates at  $\lambda_2 \approx R_0 (fN)^{1/4}$ . The adsorbed layer at distances  $z < \lambda_2$  can be viewed as a self-similar pseudo-brush of stretched polydisperse loops. The stretching of a blob

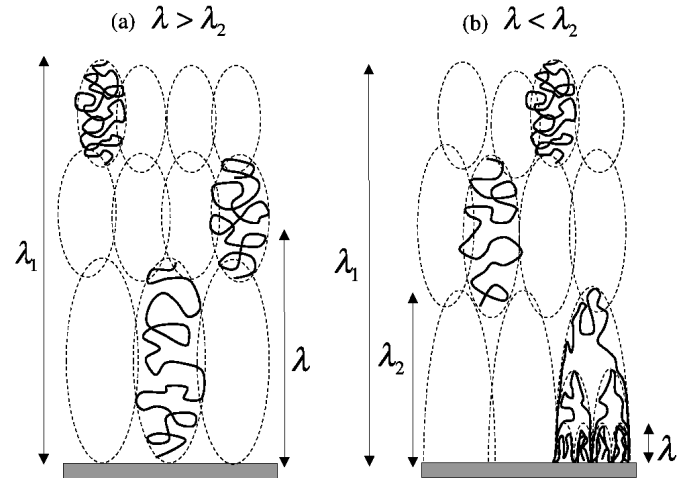


Fig. 6. Schematic sketch of the configurations of polyampholyte chains in the adsorbed layers. (a) Multilayer of stretched chains. (b) Self-similar stretched pseudo-brush at distances from the surface  $z < \lambda_2$  and multilayer of stretched chains at  $\lambda_2 < z < \lambda_1$ .

of size  $z$  containing  $g(z)$  monomers can be estimated by balancing the elastic energy  $k_B T z^2 = (a^2 g(z))$  with the polarization energy  $e f g(z) z E(z)$ . For  $z > \lambda$  the electric field is  $E(z) \approx e / (\lambda_B z)$ . The equilibrium density profile is given by:

$$c(z) \approx a^{-3} \frac{a f^{1/3}}{z + \lambda} \quad (8)$$

For  $z > z_2$ , the concentration profile is still given by equation (7). The total thickness of the adsorbed layer is

1. iii)  $z_0 > z_3$ . The size of the polyampholyte molecules in the first layer is  $z_2$ , but these chains are self-similarly stretched at all length scales between  $z_3$  and  $z_2$ . In the layer of thickness  $z_3$  near the wall the monomer concentration is constant and proportional to  $a^3 f^{1/2}$ . At distances between  $z_2$  and  $z_1$  one finds a multibrush of stretched chains.

### 3.3 Loop size distribution inside the pseudo-brush for $z_2 < z_0 < z_3$

We derive in this section the loop size distribution in the regime of interest for our experiment. The same treatment can be used to obtain the loop size distribution in the other regimes.

We consider a layer of thickness  $dz$  located at a distance  $z$  from the charged surface; the number of monomers (per unit area) in this layer is [24]:

$$c(z) dz = p(n) dn \quad (9)$$

where  $c(z)$  is the monomer concentration and  $p(n)$  the probability (per unit area) that a monomer belongs to a loop comprising more than  $n$  monomers. The loop size distribution  $S(n)$ , probability to find a loop with  $n$  monomers, is then derived from  $p(n)$  by:

$$S(n) = \frac{\partial p}{\partial n} \quad (10)$$

The relation between  $z$  and  $n$  is found by balancing the elastic energy of a strand of size  $z$  containing  $n$  monomers and its polarization energy in the electric field  $E(z)$ :

$$\frac{k_B T}{na^2} z^2 \sim \frac{e_0}{\epsilon} \frac{1}{z + z_0} e(fn)^{1/2} z \quad (11)$$

leading to:

$$z(z + z_0) \sim n^{3/2} \quad (12)$$

Using equation (8) for  $c(z)$ , we obtain  $S(n) \sim n^{-4/3} n^{-1/2}$  for  $z < z_0$ , and  $S(n) \sim n^{-3/2}$  for  $z_0 < z < z_2$ . These two asymptotic expressions of  $S(n)$  can be recast into a single formula:

$$S(n) \sim n^{1/2} (g + n)^{-1} \quad (13)$$

where  $g$ , defined by equation (6), is the mean number of monomers in a strand of size  $z_0$ . The polyampholytes located at distance  $z > z_2$  are not adsorbed directly on the surface and should not be stretched in the AFM experiments; they thus do not participate to the loop size distribution. This loop size distribution (13) is identical to the one derived by Dobrynin et al [25] when  $n > g$ ; but for  $n < g$ , we find a power-law profile instead of a constant loop size, although we have to assume that all chains fold back for  $z = z_0$ .

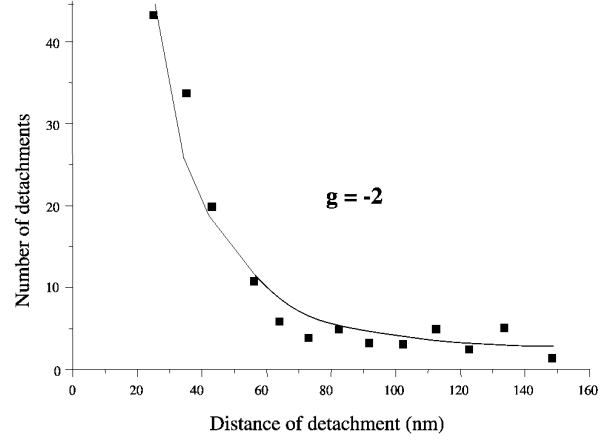


Fig. 7. Loop size distribution on a charged surface obtained with  $\text{HS}-(\text{CH}_2)_2-\text{SO}_3^- \text{Na}^+ / \text{HS}-(\text{CH}_2)_2-\text{CH}_3 = 10 \text{ \% mol/mol}$ . The full line represents the fit of the data using Eq. 1.

## 4 Results and discussion

Images obtained by AFM on the  $\text{HS}-(\text{CH}_2)_2-(\text{CF}_2)_9-\text{CF}_3$  monolayer showed a remarkably ordered 2D hexagonal lattice with a lattice constant equal to  $0.59 \text{ nm}$  on  $\text{Au}(111)/\text{mica}$  [26]; the surface density is then  $3.3 \cdot 10^{18} \text{ thiols/m}^2$ . Keeping the same value for our systems and making the assumption that the ratio of charged thiols to (charged + neutral) thiols on the gold surface remains equal to the ratio of charged thiols to (charged + neutral) thiols in the bulk solution used to process the gold surface (a very strong assumption indeed), we can estimate the surface charge density  $\sigma_0$  for the various substrates. Using the estimated values of  $z_1$ ,  $z_2$  and  $z_3$  of Section 3, it appears that our experiments are performed in the fence regime. This is justified later on Figure 11 and allows us to process our data according to the theoretical analysis exposed in 3.3. The last assumption supposes that there is no differential adsorption of the two thiols on gold.

### 4.1 Loop size distribution on $\text{HS}-(\text{CH}_2)_2-\text{SO}_3^- / \text{HS}-(\text{CH}_2)_2-\text{CH}_3$

The loop size distribution is shown on Figure 7.

We find from the numerical fit that  $g' \approx 0$  which means that no monomers are adsorbed in the layer of thickness  $z_0$ . The loop size distribution  $S(n)$  scales as  $n^{-3/2}$  as in the studies of neutral polymers reported in [14,15]. In fact, we have checked that the polyacrylamide homopolymer adsorbs on a surface covered by  $\text{HS}-(\text{CH}_2)_2-\text{CH}_3$ ; short-chain thiols form less dense monolayers than long-chain thiols [7] and are not efficient enough to prevent the polyampholyte adsorption; short-chain neutral thiols are thus not good candidates to investigate electrostatic effects.

#### 4.2 Loop size distribution on $\text{HS}-(\text{CH}_2)_2-\text{SO}_3^-/\text{HS}-(\text{CH}_2)_2-(\text{CF}_2)_7-\text{CF}_3$

Giving up with  $\text{HS}-(\text{CH}_2)_2-\text{CH}_3$ , we turned to  $\text{HS}-(\text{CH}_2)_2-(\text{CF}_2)_7-\text{CF}_3$  because of its longer chains and enhanced hydrophobicity. We have first checked that polyacrylamide does not adsorb on the fluorinated thiols: no detachment peak has been observed on the force curves. We cannot of course rule out from this observation that the polyampholyte cannot adsorb by non-electrostatic interactions between the fluorinated thiols and the chain skeleton; this possibility has not been investigated. On the other hand, polyacrylamide adsorbs on a surface covered with  $\text{HS}-(\text{CH}_2)_2-\text{SO}_3^-$ , certainly via van der Waals interactions with the underlying gold surface, and consequently the polyampholyte also adsorbs. In order to favour the electrostatic interactions between the charged monomers and the surface against the hydrogen bonds between acrylamide and the charged thiols, weakly charged surfaces have been prepared with millimolar solutions of thiol mixtures  $\text{HS}-(\text{CH}_2)_2-\text{SO}_3^-/\text{HS}-(\text{CH}_2)_2-(\text{CF}_2)_7-\text{CF}_3$  with molar ratios 0.1, 0.3, 1 and 3 %. For the two extreme cases, the loop size distribution and the fit given by equation (1) are shown on Figures 8 and 9.

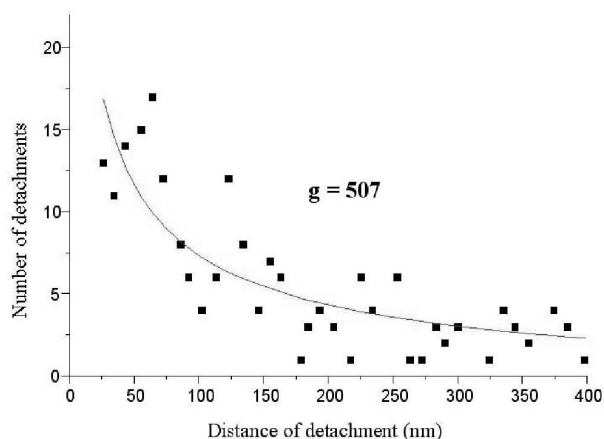


Fig. 8. Loop size distribution on a charged surface prepared with  $\text{HS}-(\text{CH}_2)_2-\text{SO}_3^- \text{Na}^+/\text{HS}-(\text{CH}_2)_2-(\text{CF}_2)_7-\text{CF}_3 = 0.1 \%$  mol/mol. The full line represents the fit of the data using Eq. 1.

For each type of surface (0.1, 0.3, 1 and 3 %), experiments have been repeated with four different substrates and the results of the fit (using Eq. 1) are given in Table 2. The different results obtained show that there is a charge effect. We can deduce that the salt initially added to dissolve the polyampholyte chains has been effectively removed from the adsorbed layer after rinsing, otherwise the field at the surface would be screened after less than 1 nm (for an electrolyte concentration of  $0.15 \text{ mol l}^{-1}$ ) and then the loop size distributions for different surfaces would be identical. Moreover, the preferential adsorption of one thiol in comparison with the other is limited, otherwise the surfaces would be covered with the same type

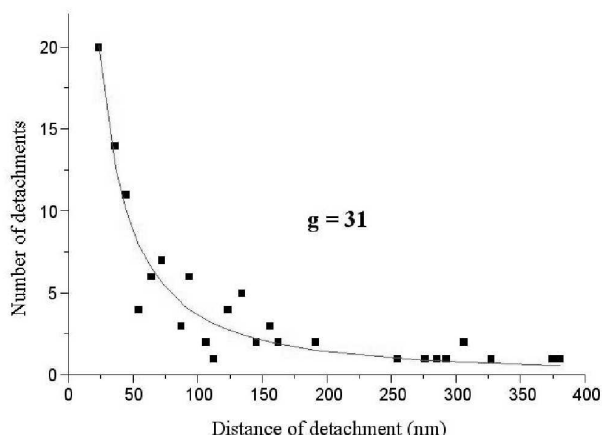


Fig. 9. Loop size distribution on a charged surface prepared with  $\text{HS}-(\text{CH}_2)_2-\text{SO}_3^- \text{Na}^+/\text{HS}-(\text{CH}_2)_2-(\text{CF}_2)_7-\text{CF}_3 = 3 \%$  mol/mol. The full line represents the fit of the data using Eq. 1.

% of charged thiol	0.1	0.3	1	3
Expt. # 1	466	170	91	31
Expt. # 2	507	70	36	22
Expt. # 3	1051	302	132	96
Expt. # 4	666	395	22	4
$\langle g \rangle$	672	234	70	38
$\langle g^2 \rangle$	231	124	44	35

Table 2. Fitted values of  $g$  for 4 different experiments with mean value  $\langle g \rangle$  and standard deviation  $\langle g^2 \rangle$ .

of thiol and there would not be any charge effect. This observation does not however allow to conclude that the rate of charged thiols at the surface is the same as the one in volume.

The results for the mean number  $\langle g \rangle$  of monomers in a loop are also plotted on Figure 10 taking the standard deviation as experimental bars.

Figure 11 shows that the AFM experiments are in the fence regime; as predicted by theory, the number  $g$  of monomers in a loop decreases with the surface charge.  $g$  scales like the ratio of charged/neutral thiols to the  $-0.86$  power; however, it seems difficult to compare it to the exponent  $-1.33$  given by Eq. 6, because the theoretical exponent links  $g$  to the surface charge and not the bulk fraction of charged thiol.

#### 4.3 Contact angle and electrokinetics measurements

Contact angles and potential for the charged surfaces made with  $\text{HS}-(\text{CH}_2)_2-\text{SO}_3^-/\text{HS}-(\text{CH}_2)_2-(\text{CF}_2)_7-\text{CF}_3$  are presented on Figure 12.

The values of  $\phi$  obtained for the monolayer of fluorinated thiols ( $-37$  and  $-39 \text{ mV}$ ) are close to the value measured by Chibowski and Waksmunk for polytetrafluoroethylene  $(\text{CF}_2)_n$  [27]. In bidistilled water, they indeed

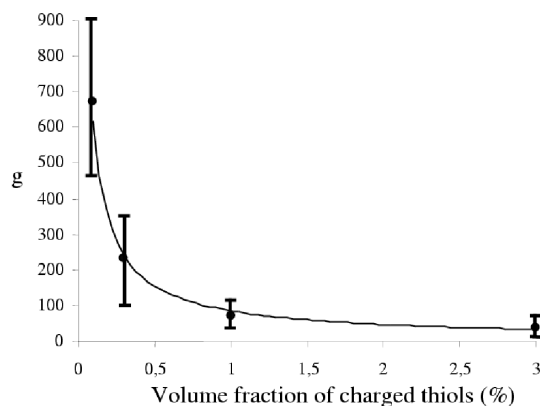


Fig. 10. Mean number  $\langle g \rangle$  of monomers in a loop against the molar ratio of charged/(charged + neutral) thiols in volume. The full line is a power law fit (see text).

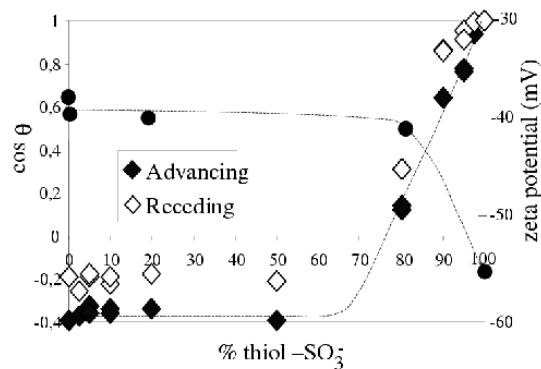


Fig. 12. Water contact angles ( $\theta$ ) and zeta potential ( $\zeta$ ) on  $\text{HS}-(\text{CH}_2)_2-\text{SO}_3^-/\text{HS}-(\text{CH}_2)_2-(\text{CF}_2)_7-\text{CF}_3$  charged surfaces.

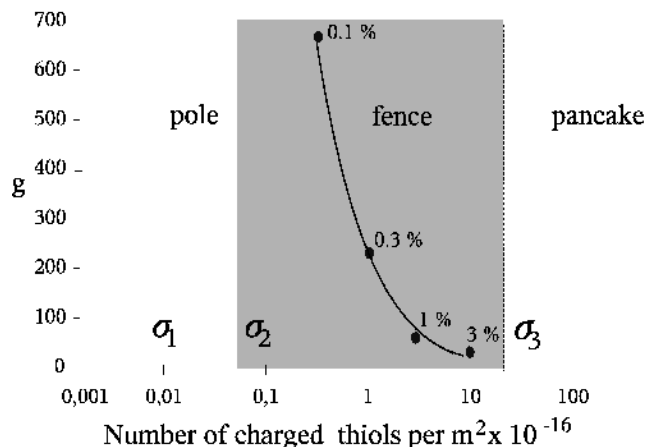


Fig. 11. The various adsorption regimes of a polyampholyte on a charged surface along with the number  $g$  of monomers in a loop versus the volume fraction of charged thiols in the adsorption solution.

found a potential equal to  $-46.6 \text{ mV}$ . The potential of the monolayer of charged thiols,  $-55 \text{ mV}$ , can be compared to that of a surface covered by mercaptopropionic acid ( $\text{HS}-(\text{CH}_2)_2-\text{COOH}$ ). By atomic force measurements in a  $10^{-3} \text{ mol l}^{-1} \text{ KCl}$  aqueous solution, Hu and Brad [28] determined the potential  $\phi_d$  above the counterion layer of this surface;  $\phi_d$  is indeed close to [22]. At  $\text{pH} > 10$ , the acid is completely dissociated, and the potential  $\phi_d$  was  $-62 \text{ mV}$ , which is compatible with the streaming current measurement.

Figure 12 shows that  $\cos \theta$  and  $\zeta$  are relatively well correlated: their values are hardly modified for a bulk fraction of charged thiol lower than 70–75 %, and then strongly change. The contact angle and the zeta potential are thus linked to the same phenomenon. The plateau can be explained by i) a preferential adsorption of the uncharged thiol, ii) a phase separation between the two types of thiols, or iii) the conformations of the thiol alkyl chains. The first hypothesis is refuted by the AFM experiments,

which show a difference between the surfaces in the region of the plateau (0.1 – 3 %). We have not performed AFM imaging to investigate the second hypothesis and the possible presence of islands resulting from phase separation. Anyway the contact angle hysteresis  $\cos \theta_r - \cos \theta_a$  is limited and identical to the one of a pure monolayer of uncharged thiols, which is a very good indication of an homogeneous surface; the zeta potential would also be extremely sensitive to the presence of charged islands. The third hypothesis seems to be the most likely. As shown by Figure 13, the  $\text{HS}-(\text{CH}_2)_2-\text{SO}_3^-$  thiols are much smaller than the uncharged ones, and the charges that they carry are hidden by the long neutral chains, which decreases their influence by a screening effect: the local reduced dielectric constant should also decrease the dissociation constant of the sulfonic groups of the smaller thiols, with the effect of a smaller effective smaller charge. This remains very schematic, since thiolated chains can be tilted on the surface and the long chains are unlikely to be in an all-trans conformation. However, AFM images of a monolayer of the uncharged thiol have revealed extended conformations with a tilt angle of  $22^\circ$  [29].

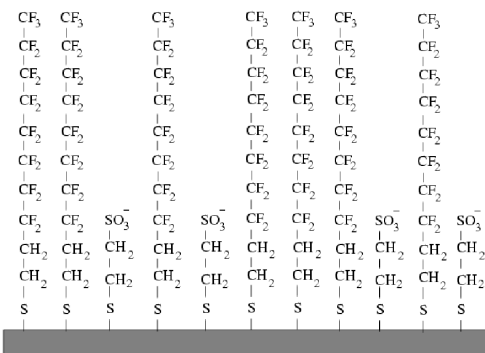


Fig. 13. Schematic distribution of  $\text{HS}-(\text{CH}_2)_2-\text{SO}_3^- \text{Na}^+$  and  $\text{HS}-(\text{CH}_2)_2-(\text{CF}_2)_7-\text{CF}_3$  on gold.



Figure 14 represents data obtained by A.-L. Bernard, who studied the surfaces  $\text{HS}-(\text{CH}_2)_2-\text{SO}_3^-/\text{HS}-(\text{CH}_2)_2-\text{CH}_3$  [30]. Contrary to the former situation, the variation of  $\cos \theta$  with respect to the percentage of charged thiols in the bulk is nearly linear, except for highly charged surfaces. The two thiolated molecules have the same length and there is no screening effect.

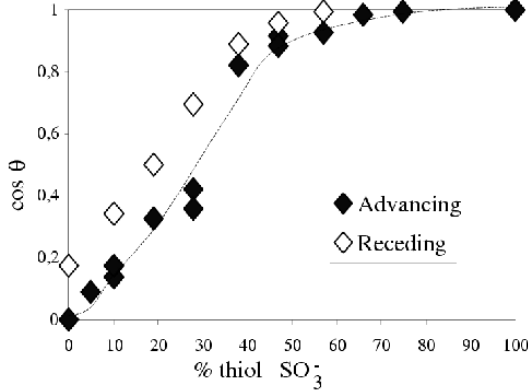


Fig. 14. Contact angle of water on a  $\text{HS}-(\text{CH}_2)_2-\text{SO}_3^-/\text{HS}-(\text{CH}_2)_2-\text{CH}_3$  monolayer (after [30]).

#### 4.4 Interpretation

A striking feature of Figure 12 is the non-zero value of the potential of the monolayer of fluorinated thiols, which are neutral molecules. Similar streaming current measurements on a monolayer of octadecanethiol [31] have showed that the potential varies with pH and salt concentration. The proposed explanation is a preferential adsorption of the hydroxide ions on the surface. In the case of the fluorinated monolayer, a preferential adsorption of anions certainly takes place, but it is difficult to decide whether the adsorbing ions are  $\text{OH}^-$  or  $\text{Cl}^-$ . The phenomenon is sketched on Figure 15. The potential is approximately equal to the potential  $\psi_d$  at the outer Helmholtz plane (OHP) and thus non-negligible due to the adsorption of anions, whereas the surface potential  $\psi_0$  remains weak [22].

The surface charge  $\sigma_d$  of the OHP plane close to the monolayer of charged thiols can be obtained with the hypothesis  $\psi_d \approx \zeta$  and the relation given by the Gouy-Chapman-Stern-Grahm theory:  $\sigma_d = 4\epsilon_0 \epsilon \sinh(e\psi_d/2k_B T)$  where  $c$  is the salt concentration, and  $\lambda_D$  the Debye length [22]. In our streaming current measurements on a monolayer of charged thiols,  $c = 10^{-3} \text{ mol l}^{-1}$ ,  $\lambda_D = 10 \text{ nm}$ ,  $\psi_d = -55 \text{ mV}$ . The obtained value  $\sigma_d = 4.9 \cdot 10^{-3} \text{ C m}^{-2}$  corresponds to a charge density equal to  $3.1 \cdot 10^{16}$  negative charges /  $\text{m}^2$ , much lower than the surface density expected for a monolayer of charged thiols: low energy helium diffraction on a  $\text{HS}-(\text{CH}_2)_9-\text{CH}_3$  monolayer [32] and surface acoustic wave studies on a  $\text{HS}-(\text{CH}_2)_6-\text{CH}_3$  monolayer [33] both established that the surface density of

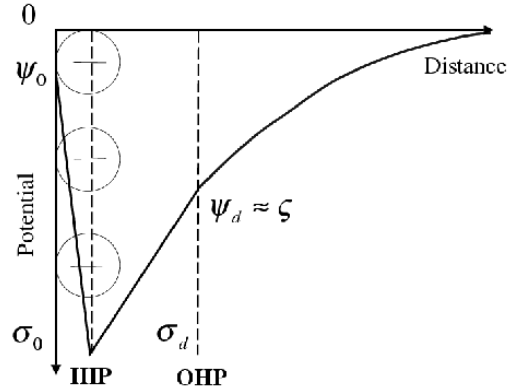


Fig. 15. Preferential adsorption of anions on a weakly charged surface; electrostatic potential profile in solution. The inner Helmholtz plane (IHP) is defined by the plane of adsorption of desolvated ions and the outer Helmholtz plane (OHP) by the plane for which the solvated ions are closest to the surface.

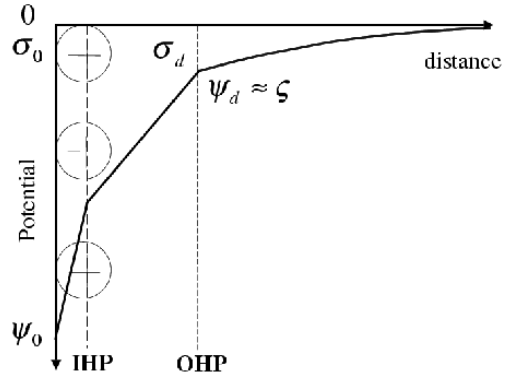


Fig. 16. Screening by counterions of a highly charged surface; electrostatic potential profile in solution.

the molecules of the thiolated monolayer is around  $5 \cdot 10^{18}$  thiols /  $\text{m}^2$ . If we suppose that the density is the same for the charged thiol monolayer, the large difference between this value and the former charge density implies a strong screening by the counterions (cations) in solution, represented on Figure 16. A similar effect was also inferred by Hu and Hard after AFM experiments on thiol monolayers [34]. We would like to stress here that it is anyway difficult to determine the actual charge that rules the electric potential of a charged surface. The determination of the charge is in fact model-dependent; the actual charge density is likely to be between the values estimated from direct (crystallographic) measurements (such as AFM [26]) and electrokinetic measurements.

Concerning the surfaces used in AFM experiments (0.1, 0.3, 1 and 3 % of charged thiols in the bulk), contact angle and electrokinetics measurements do not show any difference with respect to a monolayer of 100 % neutral fluorinated thiols (see Figure 12):  $\psi = 115^\circ$  and  $\psi = 38 \text{ mV}$ . The study of the detachment distances in AFM experiments have however revealed a charge effect in qualita-

tive agreement with the theory. These apparently contradictory observations can be explained by making the following assumption: the few short-chain charged thiols are hidden by the long fluorinated ones. Contact angle and electrokinetics measurements give then the feeling that these surfaces are covered by a monolayer of neutral thiols. These measurements are indeed realized at a mesoscopic scale, whereas the AFM ones are realized at a microscopic scale. Even if the contact angle and the zeta potential see only the neutral fluorinated thiols, polyampholytes have the ability to find their way between them to adsorb on the charged thiols (Figure 17).

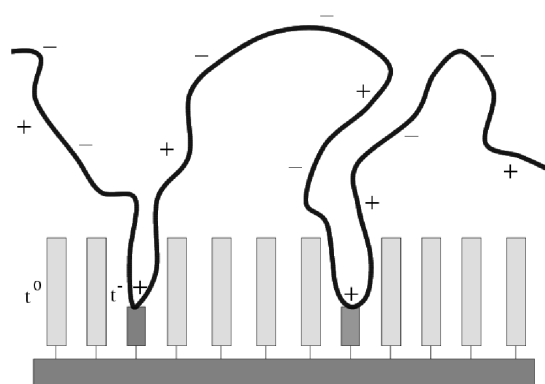


Fig. 17. Schematic sketch of the adsorption of the polyampholyte on a  $\text{HS}-(\text{CH}_2)_2-\text{SO}_3^- \text{Na}^+ / \text{HS}-(\text{CH}_2)_2-(\text{CF}_2)_7-\text{CF}_3$  monolayer.

## 5 Conclusion

The adsorption of a polyampholyte has been studied on various  $\text{HS}-(\text{CH}_2)_2-\text{SO}_3^- / \text{HS}-(\text{CH}_2)_2-(\text{CF}_2)_7-\text{CF}_3$  monolayers by AFM. The statistical analysis of the loop size distribution in the adsorbed layer reveals that the number of monomers in a loop decreases, in qualitative agreement with theoretical predictions [5, 6]. In order to measure the charge density  $\sigma_0$  of the surfaces, we have performed streaming current measurements, which gave us the potential of the surfaces. Because of a phenomenon of preferential adsorption of some ions, the value of  $\sigma_0$  could not be deduced from  $\zeta$ . For instance, the existence of a non-zero potential on the monolayer of fluorinated thiols is difficult to interpret; an explanation could be that the bond between the fluorocarbonated part of the thiol and its hydrocarbonated part creates a strong dipole [35]; this could attract anions of the electrolyte by induced-type interactions. The dipoles oriented in the bonds  $-\text{CH}_2-\text{CF}_2-$  moreover constitute a layer of dipoles which could contribute to this attraction.

The contact angle and potential measurements are well correlated, and give the same value for the monolayer of fluorinated thiols than for weakly charged surfaces.

AFM experiments on these surfaces however show different structures of the polyampholyte adsorbed layer. This apparent paradox is explained by the following interpretation: the short-chain charged thiols are hidden by the long-chain fluorinated ones, but the polyampholyte has the ability to find its way between them to adsorb. This hypothesis could be checked by infrared or Raman surface spectrophotometry and, if confirmed, could lead to interesting applications, such as the recognition by charged polymers of charged groups which are undetectable at a mesoscopic scale by a simple wetting or electrokinetics study.

## 6 Acknowledgments

The authors are thankful to Drs. Françoise Candau, Franck Clément, Georges Debregas, Albert Johnner, Marie-Pierre Kraft, Hans Lyklema, Philippe Mesini, Joseph Selb and Tim Senden for fruitful discussions.

## References

1. Blaakmeer J., Cohen Stuart M. A., and Fleer G. J. *J. Colloid Interface Sci.*, 140:314, 1990.
2. Neyret S., Ouali L., Candau F., and Peerkom E. *J. Colloid Interface Sci.*, 176:86, 1995.
3. Kato T., Kawaguchi M., Takahashi A., Takayuki O., and Tanaka H. *Langmuir*, 15:4302, 1999.
4. Le Berre F., Malmsten M., and Blomberg E. *Langmuir*, 17:699, 2001.
5. Dobrynin A. V., Rubinstein M., and J.-F. Joanny. *Macromolecules*, 30:4332, 1997.
6. Dobrynin A. V., Oubukhov S. P., and Rubinstein M. *Macromolecules*, 32:5689, 1999.
7. Bain C. D., Troughton E. B., Tao Y. T., Evall J., Whitesides G. M., and Nuzzo R. G. *J. Am. Chem. Soc.*, 111:321, 1989.
8. Neyret S., Candau F., and Selb J. *Acta Polymer*, 47:323, 1996.
9. Skouri M., Munch J.-P., Candau S. J., Neyret S., and Candau F. *Macromolecules*, 27:69, 1994.
10. Neyret S. PhD thesis, Université Louis Pasteur, Strasbourg, 1995.
11. Netz R. and Joanny J.-F. *Macromolecules*, 31:5123, 1998.
12. Brandrup J., Immergut E. H., and Grulke E. A., editors. *Polymer Handbook*. John Wiley and Sons, New York, 1999.
13. Dummond C. J. and Senden T. J. *Coll. Interf. A*, 87:217, 1994.
14. Senden T. J., diMéglio J.-M., and Auroy P. *Eur. Phys. J. B*, 3:211, 1998.
15. Senden T. J., diMéglio J.-M., and Silberzan I. *Comptes Rendus Acad. Sci. IV*, 1:1143, 2000.
16. Smith S., Finzi L., and Bustamante C. *Science*, 258:1122, 1992.
17. Bustamante C., Marko J. K., Siggia E. D., and Smith S. *Science*, 265:1599, 1994.
18. Joanny J.-F. and de Gennes P.-G. *J. Chem. Phys.*, 81:552, 1984.
19. diMéglio J.-M. and Quere D. *Europhys. Lett.*, 11:163, 1990.

20. diMaggio J.M. *Europhys. Lett.*, 17:607, 1992.
21. Hurd R.M. and Hackerman N. *Electrochem. Soc. J.*, 102:594, 1955.
22. Hunter R.J. *Zeta potential in colloid science*. Academic Press, London, 1981.
23. Israelachvili J. *Intermolecular and Surface Forces*. Academic Press, London, 1985.
24. de Gennes P.-G. *C.R. Acad. Sci. Serie II*, 294:1317, 1982.
25. Dobrynin A.V., Zhulina E.B., and Rubinstein M. *Macromolecules*, 34:627, 2001.
26. Tamada K., Ishida T., Knoll W., Fukushima H., Colorado, Jr. R., Graupe M., Shmakova O.E., and Lee T.R. *Langmuir*, 17:1913, 2001.
27. Chibowski E. and Waksundzki J. *Colloid Interface Sci.*, 66:213, 1978.
28. Hu K. and Bard A.J. *Langmuir*, 13:5114, 1997.
29. Naud C., Calas P., and Commeyras A. *Langmuir*, 17:4851, 2001.
30. Bernard A.-L. *PhD thesis, Université Pierre et Marie Curie, Paris*, 1999.
31. Schweiss R., Wezel P.B., Werner C., and Knoll W. *Langmuir*, 17:4304, 2001.
32. Camillone N., Chidsey C.E.D., Gan-Yu Liu T.M., Putvinisky T.M., and Scoles G. *J. Chem. Phys.*, 94:8493, 1991.
33. Thomas R.C., Sun L., Crook R.M., and Ricco A.J. *Langmuir*, 7:620, 1991.
34. Hu K. and Bard A.J. *Langmuir*, 14:4790, 1998.
35. Graupe M., Takenaga M., Koini T., Colorado Jr. R., and Lee T.R. *J. Am. Chem. Soc.*, 121:3222, 1999.